Deformable registration for integration of MRI/MRSI information in TRUS-guided prostate biopsy

Wei Shao[a], Ruoyun Wu[b], Choon Hua Thng[c], Keck Voon Ling[a], Henry Sun Sien Ho[d], Christopher Wai Sam Cheng[d], and Wan Sing Ng[b]

[a] School of Electrical and Eletronic Engineering, Nanyang Technological University
50 Nanyang Avenue, Singapore
[b] School of Mechanical and Production Engineering, Nanyang Technological University
50 Nanyang Avenue, Singapore
[c] Department of Oncologic Imaging, National Cancer Centre
11 Hospital Drive, Singapore
[d] Department of Urology, Singapore General Hospital
11 Hospital Drive, Singapore

ABSTRACT

Prostate cancer has been ranked as the second leading cause of cancer death in men. The existence of cancer in prostate is usually examined by a biopsy procedure under the transrectal ultrasound (TRUS) guidance. Development of a prostate biopsy robotics can alleviate urologists' labor and guarantee accuracy. However, it is usually impossible to identify cancer region in the noisy ultrasound images, thus leading to a random biopsy protocol for prostate. It is being recognized that Magnetic Resonance Imaging (MRI) and Magnetic Resonance Spectroscopy Imaging (MRSI) techniques are potential to diagnose cancer distribution in prostate. So navigating the biopsy needle towards those cancer-suspected sites could improve the cancer detection rate and reduce the possibility of false negative diagnosis results. As the prostate usually deforms under the different rectal filling of probes and change of patient postures, a deformable registration scheme is implemented for the integration of the pre-operative MRI/MRSI information with the intra-operative TRUS images. A framework including a global rigid alignment and a sequent non-rigid transformation was described in this paper to match the cross-modal prostate surfaces and thereafter their volumes. For validation, an elastic prostate phantom that simulated the human condition was built up, with fiducial markers implanted inside the phantom prostate as the "ground truth". It shows that our method can achieve at least 30% improvement in accuracy compared with an affine transformation. Preliminary study was also conducted on patient data but with visual assessments presented only due to the current lack of "ground truth".

Keywords: Image registration, magnetic resonance spectroscopy, transrectal ultrasound

1. INTRODUCTION

Prostate cancer is ranked as the most common internal (non-skin) cancer and the second leading cause of cancer deaths in men, only after lung cancer. The American Cancer Society estimated that there would be about 232,090 new cases of prostate cancer in the United States in the year 2005 and about 30,350 men would die of this disease[1]. Early detection of prostate cancer can gain more chances of successful treatment. However, there are no clear symptoms of prostate cancer until it is quite advanced. This makes it quite different from breast cancer or testicular cancer in which regular self examination can be important in finding early signs of the disease.

Digital rectal examination (DRE) and prostate-specific antigen (PSA) blood test are routine screening methods used in the prostate cancer diagnosis. When a patient had an abnormal DRE and/or an elevated PSA level (> 4ng/ml), he is suspected to have a cancerous prostate and a needle biopsy is recommended. Transrectal ultrasound (TRUS) is widely used as the guiding system during the urologist-manipulated biopsy, due to its safety, low cost and simple of use. To alleviate the labor of urologists and ensure biopsy accuracy, a prototype robotic system for prostate biopsy was developed in our group. A TRUS system was also integrated as the guidance tool. However, recognition of malignant

Medical Imaging 2005: Image Processing, edited by J. Michael Fitzpatrick, Joseph M. Reinhardt, Proc. of SPIE Vol. 5747 (SPIE, Bellingham, WA, 2005)
1605-7422/05/$15 · doi: 10.1117/12.594897

tumor directly from the poor-quality ultrasound images is nearly impossible for the urologists, and even worse for the robotic system. Practically, the biopsy cores are selected either randomly or uniformly distributed within the gland, e.g., like the sextant or 10-core biopsy protocols[2-3]. As the number of biopsy cores is limited and the random cores may miss the cancer region, these biopsy protocols may lead to inaccurate or false negative results, i.e., informing a patient free of cancer but in fact not.

Amelioration to this problem is to make the biopsy needle toward areas where the cancer is mostly suspected. Such *a prior* knowledge could be obtained from a statistical atlas or a patient-specific model on the prostate cancer distribution. Statistical atlases of prostate cancer distribution[4-5] are applicable to prostate population, but their detection sensitivity for individual subject is still unpredictable. Compared with the universal models, the patient-specific model established from pre-operative information of this individual seems to be superior in providing more liable estimation. Some higher resolution imaging or biochemical imaging techniques, process the potential to present the information of suspected prostate cancer distribution. For instance, Magnetic Resonance Imaging (MRI) is a well-established technique that produces high-contrast images regarding to tissue components. When the cancer carcinoma grow to some extent, it is possible for experienced radiologists to distinguish them with the normal regions, as the cancer is usually identified as an area of low signal intensity within the peripheral zone on T2-weighted images. As an extension of MRI, Magnetic resonance spectrscopy imaging (MRSI) is a method of obtaining biochemical information from a series of local spectrum analysis over the prostate gland. Significantly higher choline/creatinine levels and lower citrate levels are usually obtained in regions of cancer compared with benign and normal prostatic tissue, so the ratio of these metabolites (choline/creatinine to citrate) in a local region could indicate a positive suspect. There are already plenty of studies on MRI/MRSI ability in predicting the cancer existence in the prostate[3,6]. This paper will discuss how the MRI/MRSI information is registered with the intra-operative TRUS images in the prostate biopsy.

2. BACKGROUND

Image registration is a critical issue addressed in the integration of MRI/MRSI information with TRUS images. It is the determination of a spatial transformation between two image spaces, which maps points of an image onto corresponding points of the other image. Registration of 3D images is a prerequisite to merge the complementary information available in multi-modality imagery (e.g., MRI/MRSI and TRUS), to study the pathological evolution of the same patient at different times, to relate preoperative images or surgical plans to the physical reality of the patient in the operating room during image-guided surgery or in the treatment suite during radiotherapy, to compare an individual with a standard atlas or among different patients.

In many applications, a rigid transformation is sufficient to describe the spatial relationship between two images, given that no deformation occurs. However in this application, the rectum, which is just beneath the prostate, would be filled with a US probe during TRUS scanning or an endorectal coil during MRI/MRSI scanning. Compared to the status under TRUS scanning, the soft-tissue-made prostate is pushed towards the pubic bone and flattened at the posterior bottom under MRI/MRSI scanning. General pattern of the deformation could be described as that the whole gland increases at transverse dimension and decreases at anterior-posterior (AP) direction, with relatively greater decrease for peripheral zone (PZ) than for central gland (CG, including central zone, CZ, and transition zone, TZ), while no statistical change at superior-inferior (SI) direction[8]. Another cause of deformation may come from the change of patient posture between the scans. The patient was placed supinely in the closed-bore magnet for the MRI/MRSI examination, but in the TRUS-guided biopsy he was in a lithotomy position to facilitate the transperineal puncture. Furthermore, Van Herk et al[8] found that leg movement like "scissors" or left-right roll of the legs might affect the rotation of the prostate around the craniocaudal axis. Influence from the bladder filling or needle puncture were sometimes also worthy of consideration[9]. Hence, non-rigid transformation is required in this application to accommodate the variability due to motion.

Literature on image registration[10] generally falls in two categories, intensity-based and surface-based. In the application to the prostate, the former was applicable where image intensity is distinct and creditable[9,11]. The latter was usually a combination of establishment of surface correspondence and an interpolation strategy from surface to volume. A simplified assumption was made by Zaider et al[12] in the registration between the MRSI to the intraoperative-obtained US images, that points within the gland maintained the same relative position with respect to the axial contour and no displacement in the SI direction. This assumption was later improved by taking into account the proportional change with respect to the center-of-mass along the z axis (craniocaudal axis)[12]. Wu et al[11] used a polynomial form used for

describing the transformation. Xuan et al[14] proposed a finite-element surface-spine model to describe the motion of the prostate, which was governed by Lagrangian motion equations. Bharatha et al[15] also proposed a non-rigid registration method using biomechanical model with linear elasticity. Relied on manual segmentation and terrahedral meshing, the prostate were labeled with different material properties. An active surface algorithm[16] was applied to deform the extracted boundary, which was treated as an elastic membrane, iteratively to it corresponding boundary. The volumetric deformation field was solved as a boundary-value problem in finite element model (FEM). However, mesh generation is a big concern in correlating the deformable models. Crouch et al[17] addressed this problem and presented a medial model "m-rep" to the undeformed and deformed prostate. Using "m-rep", the finite element mesh generated from original image could be transferred and automatically fitted to the deformed counterpart. Of same topology, the two models directly defined a one-to-one correspondence geometrically. Solutions were then obtained by further optimization of the deformation energy over the solid entity from the initialization. Rather than linear models used before, Mohamed et al[18] built up a non-linear elastic model for patient-specific data and statistically analyzed the simulated insertion of TRUS probe in this model. The combined statistical and biomechanical model was then used for real-time tracking of deformation.

It is known although physical model can simulate the prostate deformation well, it requires tissue properties which are not readily available in reality and usually consumes large amount of computation. In addition, it usually models the prostate deformation as a boundary condition problem, therefore surface or volume correspondence is still needed to be pre-determined before hand. Hence, the solution in FEM is actually an interpolation problem from sparse displacement estimates. In this paper, we proposed to use a framework including a global rigid alignment and a sequent non-rigid transformation to match the cross-modal prostate surfaces and thereafter the volumes. Thin-plate spline[19] was employed to describe the non-rigid transformation.

3. METHODOLOGY

To spatially deform one volume with respect to the other, usually two stages were taken: firstly a rigid transformation that compensates for the global change in position and orientation, secondly a non-rigid registration that refines the transformation with more degrees of freedom (DOFs) based on local similarities. A hidden assumption of the non-rigid registration is that the transformation should vary smoothly over the entire field to avoid splitting or folding. This transformation is usually described as locally translational, i.e., as the deformation field that stores displacement vector at each node position at a dense cubic lattice. In the integration of multimodal information, information from MRI/MRSI (such as the images or the cancer distribution) will be transformed to match with the TRUS images to provide the biopsy roadmap. So the former is taken as floating while the latter remains fixed as the reference.

3.1 Global registration

Because of the speckle noise in the ultrasound images, the purely intensity-based methods are highly possible to fail in the crossmodal registration, even though the MRI image contrast is good in differentiating structural contents. Due to the same reason, it is equally infeasible to identify corresponding landmarks in US images with respect to those in MRI images. Nevertheless, the delineated prostate from MRI/MRSI images could be regarded as *a prior* knowledge of the intra-subject prostate in the US images. Provided that the deformation is small, it is reasonable to suppose the delineated prostate surface in the MRI images is generally consistent with its boundary in the US images, as the prostate appears as a relatively dark region surrounded by a bright halo, with subsequent dark regions in the US images. This idea was first proposed in our previous report[20] as an automatic surface-to-volume registration method for tracking organ in US image sequence, followed by its application to rigid registration between MRI and US images[21]. In this report, this method was employed for the global alignment of the prostate between images, based on the condition that the deformation is small.

Firstly, a set of the prostate boundary in parallel transverse MRI image planes was segmented manually. A NURBS (Non-Uniform Rational B-Spline) surface was then constructed by skinning through these contours sequentially along z axis. This surface was then denoted as a parametric representation

$$S_{MR}: \mathbf{x}_A(u,v) = [x(u,v), y(u,v), z(u,v)]^{\mathrm{T}} \quad (1)$$

where vector $\mathbf{x}_A$ represents the coordinate of surface points relative to a Euclidean space (x, y, z), with its parameter u and v related to ratio of arc length in orthogonal directions, respectively, and within range [0,1]. In the NURBS

construction, we obeyed this rule that u is parameterized within x-y plane and in clockwise (or counterclockwise) direction of the closed 2D contours and v is along the z axis that is vertical to contours. Basic idea of the surface-to-volume registration method[20] is that the floating MRI surface is registered to the intra-subject US volume by maximizing the average image gradients along the normals of the transformed floating surface. The genetic algorithm (GA)[22] was adopted for global optimization, with transformation parameters T_g encoded in the chromosome and fitness function f with respect to T_g defined as follows:

$$f(T_g) = \frac{1}{N}\sum_{k=1}^{N}\left\langle \vec{G}\left(T_g(\vec{x}_k)\right)\cdot T_g(\vec{n}_k)\right\rangle \tag{2}$$

where N stands for the number of uniformly-sampled points on the floating surface, with $\vec{x}_k$ as the coordinate of the k-th sampled point on the surface and $\vec{n}_k$ as the unit vector of the surface normal at this point, whose direction is pointing from the inside to the outside. $\vec{G}$ denotes the image gradient of the Gaussian-smoothed US volume. Operator $\langle\cdot\rangle$ denotes the inner product. If any of these points falls outside of the volume of interest, its contribution to the fitness function will be set as zero. Usually N is chosen to be around 300.

Based on its fitness function, this method locates the prostate at the boundary rather than its centroid. We have demonstrated that its registration accuracy deteriorates with the amount of deformation[21]. Therefore, if the requirement of the global alignment is emphasized on the centroid, the surface-to-surface registration method is only applicable when deformation is small, for instance, the maximum Hausdorff distance between the deformed and undeformed prostate surfaces is within 2 mm when their centroids are overlapped. Otherwise, a surface-to-surface registration method, such as the iterative closest point (ICP) algorithm[23], could be used, with the other prostate surface in US images segmented on the fly from the registered result of the surface-to-volume method.

3.2 Deformable registration

Once the overall translation and rotation was solved, the deformable registration would be applied to refine the transformation locally, i.e., by allowing for more DOFs in the transformation. Polynomial or spline is commonly used for representation of transformation. But the ability of polynomial to recover high-frequency distortion is quite limited. This is because the behavior of high-degree polynomial is unpredictable, e.g., the spurious oscillation is more likely to occur. Therefore, the thin-plate spline[19] was adopted as the radial basis function for transformation in our method.

3.2.1 Thin-plate spline

Thin-plate spline (TPS) was originally proposed by Harder et al[28] in aircraft wing designs. It was later employed to describe deformations as an interpolant that minimizes the bending energy through control points[19,25-26]. The control points, **P**, were usually chosen at feature points or landmarks. Generally, the TPS-based transformation T_g is divided into separate dimension of the space domain $\Re^d$, with each component T_i defined as a combination of M radial basis functions $\phi(r)$:

$$T_i(\mathbf{x}_A) = \sum_{j=0}^{d} c_{i,j}\mathbf{x}_A(j) + \sum_{k=1}^{M} w_{i,k}\phi\left(\left|\mathbf{x}_A - \mathbf{P}_k\right|\right), \qquad i = (1,\cdots,d) \tag{3}$$

with

$$\phi(r) = \begin{cases} r^2\log(r) & 2D \\ r & 3D \end{cases} \tag{4}$$

where the original point coordinate $\mathbf{x}_A = (x_1,\cdots,x_d)_A^T$ was augmented to homogeneous representation $\mathbf{x}_A(j) = \begin{cases} (x_j)_A & 1 \le j \le d \\ 1 & j = 0 \end{cases}$. The coefficients $c_{i,j}$ and $w_{i,k}$ characterize the affine and non-affine part of the transformation, respectively. $\mathbf{P}_k$ stands for the k-th landmark (control point) in source data. A set of $d\cdot(M+d+1)$ linear equations were determined by the interpolation condition at the control points, as well as the additional conditions that the sum of the

non-affine coefficients equals to zero, and their crossproduct with coordinates is also zero. So, the coefficient vector $W_i = (w_{i,1}, \cdots, w_{i,M})^T$ and $C_i = (c_{i,0}, \cdots, c_{i,d})^T$ is calculated by

$$\begin{cases} \Phi W_i + \mathbf{X}_A C_i = \mathbf{X}_B(i) \\ \mathbf{X}_A^T W_i = 0 \end{cases} \qquad (i = 1, \cdots, d) \tag{5}$$

where matrix Φ is composed of $\phi_{ij} = \phi(\mathbf{x}_A - \mathbf{P}_j)$, $\mathbf{X}_A$ stands for the augmented array of points in source space and $\mathbf{X}_B(i)$ represents the column vector of one component of the point array in target space. The general form of the bending energy through control points, is denoted as the functional J over the domain $\Re^d$ of dimension d and the order m of derivative[26]:

$$J_m^d(T) = \sum_{\alpha_1 + \cdots + \alpha_d = m} \frac{m!}{\alpha_1! \cdots \alpha_d!} \int \cdots \int_{\Re^d} \left(\frac{\partial^m T}{\partial x_1^{\alpha_1} \cdots \partial x_d^{\alpha_d}} \right) dx_1 \cdots dx_d \tag{6}$$

For example, in 2D space the biharmonic bending energy is given by[19]

$$\int\int_{\Re^2} \left(\left(\frac{\partial^2 T}{\partial x^2} \right)^2 + 2 \left(\frac{\partial^2 T}{\partial x \partial y} \right)^2 + \left(\frac{\partial^2 T}{\partial y^2} \right)^2 \right) dx dy \tag{7}$$

3.2.2 Surface correspondence

An assumption of the non-rigid registration was made in the coordinate system of the US images, that once the prostate has been globally rotated and translated by the previous rigid registration, the cross-plane deformation along SI direction is only scaling. Therefore, the 3D non-rigid registration is done in a multiple 2D manner, i.e., slice-by-slice. Since the radial basis function TPS was used, it is necessary to determine the pairs of control point between the source and target data. Manual selection of landmark based on intensity information[12] is infeasible here because of the poor image quality. Hence, the geometric information, such as the curvature information, as well as the arc-length-based parameterization of the pre-deformed and deformed surface, was utilized to establish the correspondence.

As introduced before, the prostate capsule in US images could be segmented based on the initialization from registered result[25]. It will be parameterized in the same way how S_{MR} was parameterized, thus yielding the surface described as S_{US}: $\mathbf{x}_B(u,v) = [x(u,v), y(u,v), z(u,v)]^T$. And the rigidly-transformed surface $T_g(S_{MR})$ will be re-parameterized to accommodate with the US image coordinate system. Once the two surfaces were parameterized in a same space, a rough one-to-one mapping T could be established on (u,v) domain[27], i.e., correspondence on parametric coordinate:

$$\mathbf{P}_k \in \{\Omega_{MR} \mid (T_g(S_{MR}) : \mathbf{x}_A(u,v))\} \xrightarrow{(u,v)} \mathbf{Q}_k \in \{\Omega_{US} \mid (S_{US} : \mathbf{x}_B(u,v))\}, \qquad \forall (u,v) \in D \tag{8}$$

where Ω_{MR} and Ω_{US} represent the respective space domain, and D is the parametric space where $0 \le u \le 1$ and $0 \le v \le 1$. This matching is actually relevant to arc length in u and v directions. Let Θ denotes the conversion from parametric coordinate (u,v) to Cartesian coordinate (x,y,z) in one NURBS surface formulation, $(x,y,z) = \Theta(u,v)$, and Θ^{-1} its reverse conversion, $(u,v) = \Theta^{-1}(x,y,z)$, the transformation T in Cartesian coordinate system could be worked out by the two point sets **P** and **Q** of same coordinate in parametric coordinate system, using TPS as the radial basis function.

However, this matching might fail for irregular shapes[28]. Solution to this problem is to take additional geometric information, such as the curvature information, into account to determine the correspondence. Once the deformation was decoupled into u- and v-space according to our assumption, some feature points were to be identified within each image plane. These prominent features can be chosen at those corner points which are mostly representative to the closed contour of the prostate shape in MRI/MRSI scanning. They are the anterior corner (AC), the posterior corner (PC), the left corner (LC) and right corner (RC) along the closed 2D contour. Not only for automatic detection, selection of control points on these corner features can also ensure maximum coverage of the prostate region.

Firstly, slice correspondence was set up by proportional scaling with respect to the centroid along the z axis (v-space). Secondly, the prominent corner points (P_{AC}, P_{PC}, P_{LC} and P_{RC}) were identified automatically in MRI data based on the Gaussian curvature calculated along contour in each slice. By connecting the respective feature points cross sections, four ridges were constructed, representing the global frame of the prostate shape. The point coordinate (x,y) on each ridge will be a function with respect to the section depth z: $(x, y) = [f_1(z), f_2(z)]$. To reduce interslice fluctuation in point identification, a low-pass filtering is applied, $(x', y') = [G_{\delta_1}(f_1(z)), G_{\delta_2}(f_2(z))]$. The smoothed ridge was then projected back to each section contour and the projection will be the updated feature points. This procedure can also be repeated until the projection distance after smoothing is within a threshold. Thirdly, the correspondent Q_{AC} and Q_{PC} points in TRUS data were still identified based on curvature and arc length information. But the correspondence of the other two features, Q_{LC} and Q_{RC}, will be determined based on arc length information, that is, proportional arc length in leget (or right) half segment. This relationship is formulated as follows:

$$u'_{LC} = u'_{PC} - \frac{u'_{PC} - \tilde{u}'_{AC}}{u_{PC} - \tilde{u}_{AC}}(u_{PC} - u_{LC}) = \Theta^{-1}(Q_{LC}) \tag{9}$$

$$u'_{RC} = u'_{PC} + \frac{\hat{u}'_{AC} - u'_{PC}}{\hat{u}_{AC} - u_{PC}}(u_{RC} - u_{PC}) = \Theta^{-1}(Q_{RC}) \tag{10}$$

where

$$\tilde{u}_{AC} = \begin{cases} u_{AC} & 0 \le u_{AC} \le 0.5 \\ u_{AC} - 1 & 0.5 \le u_{AC} \le 1 \end{cases} \tag{11}$$

$$\hat{u}_{AC} = \begin{cases} 1 + u_{AC} & 0 \le u_{AC} \le 0.5 \\ u_{AC} & 0.5 \le u_{AC} \le 1 \end{cases} \tag{12}$$

u_{PC}, u'_{PC} stands for the parametric coordinate of P_{PC} and Q_{PC}, and so on. To ensure accuracy over the prostate region, denser points were sampled along the contour, according to a criterion of uniform interval within each of the four segments partitioned by feature points. The two sets of points, **P** and **Q,** constructed the correspondence, which is proportional in z axis or v space, and piecewisely equal in u spaces (or (x,y) domain) at any z depth. The number of the sampling points within each segment was usually selected empirically, considering the balance between accuracy and computation expense.

3.2.3 Volumetric interpolation

As a radial basis function, the TPS kernel propagates the displacement vectors on sparse control points into their neighborhood. So the volumetric deformation was defined as follows, in separate x, y and z components:

$$\begin{cases} T_{x,y} = c_0 + c_x x + c_y y + \sum_{k=1}^{M} w_i \phi(|\mathbf{P}_k - (x, y)|) \\ T_z = c_z(z - z_0) \end{cases} \tag{13}$$

where the coefficients c_0,c_x, c_y and weights w_i were calculated according to Equation (5), with the basis function $\phi(r) = r^2 \log(r)$ according to Equation (6). Coefficient c_z was determined by the proportional scaling in z axis, with respect to the center of mass.

4. DATA COLLECTION AND EXPERIMENTS

4.1 Phantom study

A self-designed elastic phantom, including simulated prostate, rectum and surrounding tissues, was set up for validation purpose, as shown in Figure 1. To quantitatively evaluate the deformation of the prostate, fifteen fiducial markers were

implanted into the prostate in a regular distribution. These dummy markers were visible in MRI images so that they could be used as the "ground truth" for error estimation, but not in registration itself. The rectum was designed to be elastic also, in order to cater for the deformation caused by insertion of the imaging probe. A soft container filled with water would be placed on top of the prostate phantom during the deformation experiment to simulate the obstacles from the pubic bone (which can be seen in Figure 2).

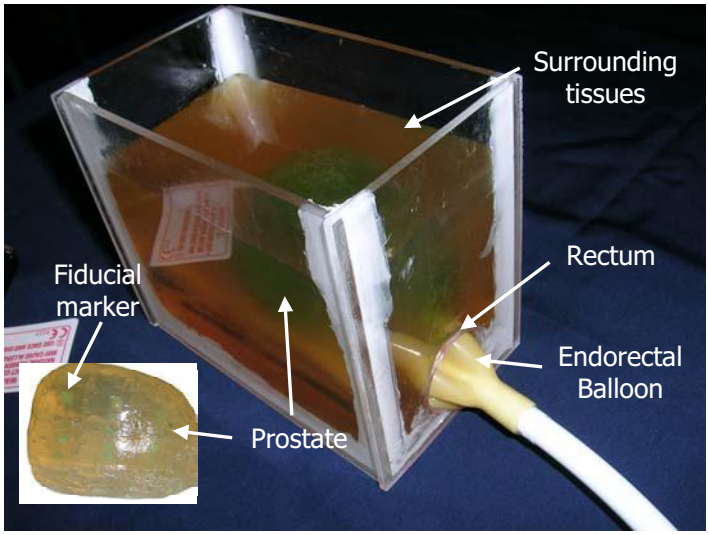

Figure 1. Self-designed prostate phantom for deformation simulation

MRI scans were performed on the phantom, without and with inflation of air into the endorectal balloon that had been inserted into the "rectum". The amount of air injected was around 40ml, same as that used in patient exams. Both MR scans were performed on 1.5 Tesla whole body GE MR systems (GE Inc). The phantom was placed in a supine position. T2-weighted fast spine-echo scanning was performed under TR/TE of ~4940.0/92.3ms, slice thickness of 3mm, and slice spacing of 0.5 mm. Imaging resolution was 256 × 256 pixels in field of view (FOV) of 12.0×12.0 mm^2. For each series, 22 slices were obtained. One simulated the patient MRSI images while the other simulated the US images. Figure 2 demonstrated acquired images and the segmented prostate capsule. It may be necessary to pre-process the MRI images for the purpose of highlighting the prostate boundary and markers.

Before the application of registration algorithm, the two image volumes were first resmapled to uniform resolution of 0.5×0.5×0.5 mm^3. Manual efforts were borrowed in the segmentation of both prostate surface. Parameters of the GA engine is set to as 600 population, 300 generation, 95% crossover ratio, 5% mutation ratio, tournament selection scheme and crowding algorithm. After the global alignment, the TPS-based transformation was established using automatically-indentified feature points. In our test, the prostate was partitioned into 30 slices along *z* depth and 20 control points per slice, where every other 4 points were uniformly sampled within each segment. Registration accuracy was evaluated as the displacement of the marker position between the reference images (undeformed) and the recovered images by transformation (deformed). Figure 3 demonstrated the calculated displacement errors of the fifteen markers, compared with the result using an affine transformation[17]. It shown that our method can achieve an accuracy of about 1.28 ± 0.50 mm (mean ± standard deviation), around 32.6% improvement compared to the accuracy of 1.90 ± 0.94 mm using affine transformation. Considering none of the knowledge within the prostate was used during the registration, we think this method was generally effective in predicting the deformation.

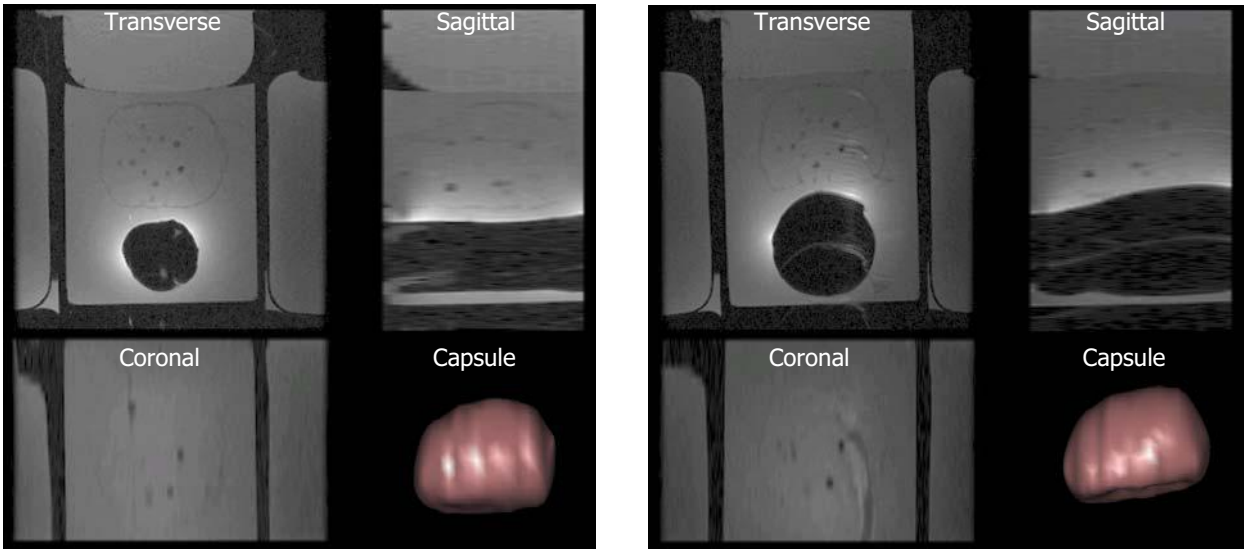

(a) (b)

Figure 2. Transverse, sagittal and coronal views of the phantom before and after deformation. (a) With endorectal coil inserted into the rectum but no air inflation. (b) With endorectal coil inserted and 40ml air inflation. Prostate capsules before and after deformation were also shown for comparison.

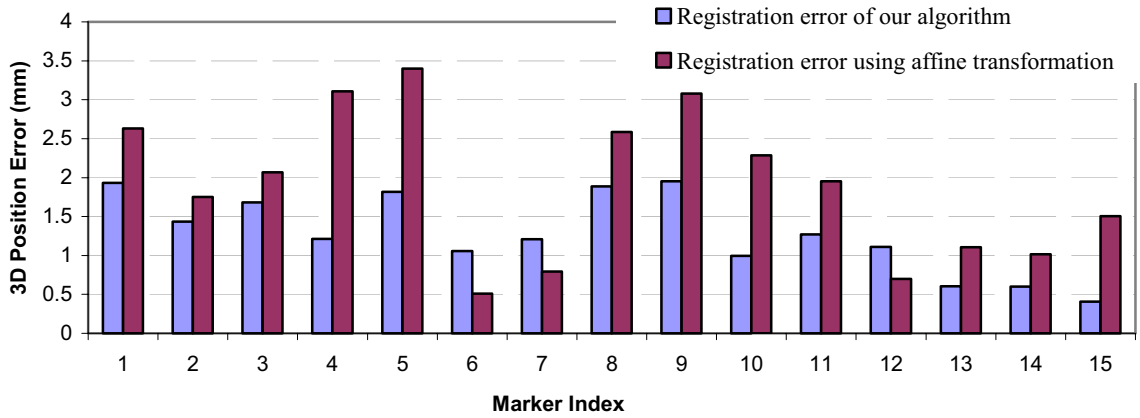

Figure 3. Displacement error of markers using affine transformation and our algorithm

4.2 Preliminary study on patient data

Same MRI machine was used for patient data collection. The endorectal FSE T2-weighted images were acquired with TR/TE of 4100-5200/-92ms, slice thickness of 3.0mm and interslice gap of 0.5mm. Image resolution is 512×512 pixels in 12.0×12.0 cm^2 FOV. The intra-operative TRUS system was Aloka SSD-1700 (Mediason Inc), which was integrated into our biopsy robotics and yielded image resolution of 0.18×0.18×1.0 mm^3. Original images were shown in Figure 4 (a) and (c), respectively.

Same paramters were used for the patient registration test. The prostate capsule in TRUS images could be segmented either manually or through algorithm. Since it was not the focus discussed here, we will inspect the registration performance regardless of segmentation errors. Based on the theory of our algorithm, it should be able to garanttee a good match on the prostate boundary, which was already seen in the experimental result by visual comparison. "Ground truth" was required for the quantitative evaluation here. But either manual selection of correspondent anatomic

landmarks or marker implantation into the patient prostate were infeasible, for the poor TRUS image contrast inside the prostate for the former, and safety concern of the patient for the latter. So we merely showed the registration results in Figure 4 for visual assessment.

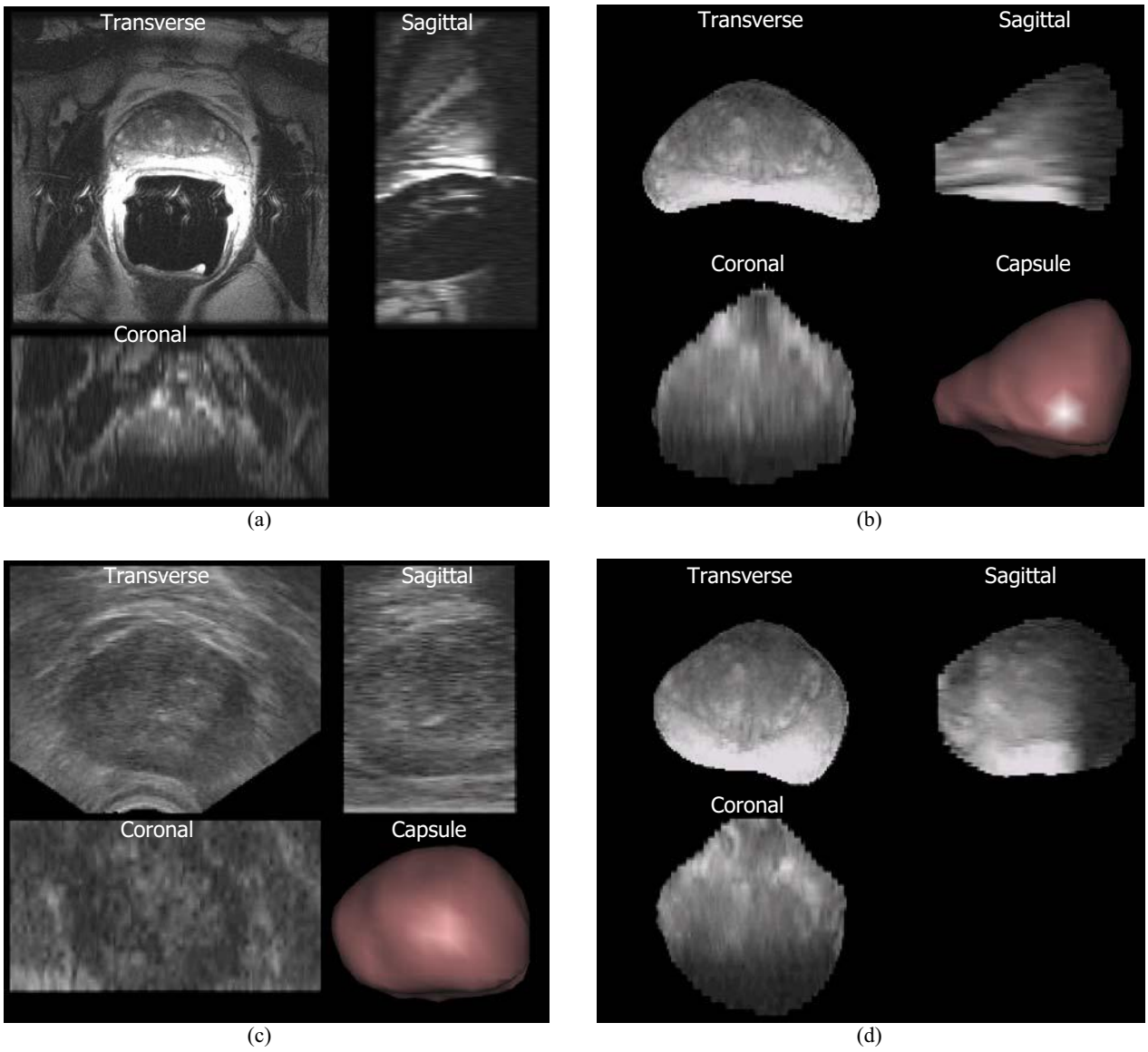

Figure 4. Registration experiment on patient data. (a) Original T2-weighted MRI images. (b) Segmented prostate from (a). (c) Original TRUS images and segmented prostate. (d) Registration result. Transformation was applied to (b), with the aim to match with (c).

5. CONCLUSIONS

In this paper, we have described a deformable registration method for the purpose of integrating the MRI/MRSI information into the TRUS-guided prostate biopsy. The suspected cancer distribution diagnosed from MRI/MRSI images, as well as the anatomic structural information provided by MRI, could lead to a targeted biopsy with higher detection rate of cancer. The framework of our method contains an initial global transformation and thereafter non-rigid matching based on surface information. Based on the geometric features on the surfaces, thin-plate spline warping is used to propagate the surface deformation to the overall volume. We also built up an elastic phantom for validation

purpose. Accuracy of this registration method was found to be around 1.28 mm, more than 30% improvement compared to that of affine transformation. However, without ready "ground truth" on real patient data at current stage, we only demonstrated preliminary result of its performance.

Future work will concentrate on the improvement of the registration accuracy, and the establishment of a credible validation system. Lack of the evidence of similarity inside the prostate capsule is a big problem for the registration. Since the condition of rectal filling affects the prostate mostly, the deformation pattern of the rectum would be helpful in predicting the deformation of the prostate. Furthermore, if the image quality of TRUS can be improved, some intensity measurements, such as mutual information, might be able to integrate with the TPS warping[29]. For the validation between MRI and TRUS images for patient data, we are hoping to implant markers into the cadaver prostate in the future. An alternative is to evaluate the accuracy by using a pair of MRI images only, with one of them simulating the deformation condition in TRUS imaging.

REFERENCE

1. American Cancer Society, Overview of Prostate Cancer: How Many Men Get Prostate Cancer, http://www.cancer.org/docroot/CRI/content/CRI_2_2_1X_How_many_men_get_prostate_cancer_36.asp?sitearea=
2. K.K. Hodge, J.E. McNeal, M.K. Terris, T.A. Stamey, Random Systematic Versus Directed Ultrasound Guided Transrectal Core Biopsies of the Prostate, *Journal of Urology*, 142(1): 71-74, 1989
3. J.S.P. Yuen, C.H. Thng, P.H. Tan, L.W. Khin, S.J.L. Phee, D. Xiao, W.K.O. Lau, W.S. Ng and C.W.S. Cheng, Endorectal Magnetic Resoance Imaging and Spectroscopy for The Detection of Tumor Foci Inmen with Prior Negative Transrectal Ultrasound Prostate Biopsy, *Journal of Urology*, 171: 1482-1486, April 2004
4. J. Zeng, J.J. Bauer, A. Sofer, X. Yao, B. Opell, W. Zhang, I.A. Sesterhenn, J.W. Moul, J. Lynch, and S.K. Mun, Distribution of Prostate Cancer for Optimized Biopsy Protocols, *International Conference on Medical Image Computing and Computer-Assisted Intervention (MICCAI'00)*, 1935: 287-296, 2000
5. D. Shen, Z. Zhao, J. Zeng, I.A. Sesterhenn, L. Sun, J.W. Moul, E.H. Herskovits, G. Fichtinger, and C. Favatzikos, Optimized Prostate Biopsy via A Statistical Atlas of Cancer Spatial Distribution, *Medical Image Analysis*, 8(2): 139-150, 2004
6. R. Bourne, P. Katelaris, S. Danieletto, T. Dzendrowskyj, P. Stanwell, and C. Mountford, Detection Of Prostate Cancer By Magnetic Resonance Imaging And Spectroscopy in vivo, *ANZ Journal of Surgery*, 73(8): 666-668, August 2003
7. R.K.T. Haken, J.D. Forman , D.K. Heimburger, A. Gerhardsson, D.L. McShan, C. Perez-Tamayo, S.L. Schoeppel, and A.S. Lichter, Treatment Planning Issues Related to Prostate Movement in Response to Differential Filling of the Rectum and Bladder, *Int J Radiat Oncol Biol Phys*, 20: 1317–1324, 1991
8. M. van Herk, A. Bluce, A.P.G. Kroes, T. Shouman, A. Touw, and J.V. Lebesque, Quantification of Organ Motion During Conformal Radiotherapy of The Prostate by Three-Dimensional Image Registration, *Int J Radiat Oncol Biol Phys*, 33: 1311–1320, 1995
9. B. Fei, C. Kemper and D.L. Wilson, A Comparative Study of Warping and Rigid Body Registration for the Prostate and Pelvic MR Volumes, *Computerized Medical Imaging and Graphics*, 27: 267-281, 2003
10. L.G.H. Derek, G.B. Philipp, H. Mark, and D. Hawkes, Medical image registration, *Phys. Med. Biol.*, 46: R1–R45, 2001
11. X. Wu, S.J. Dibiase, R. Gullapalli, and C.X. Yu, Deformable Image Registration for the Use of Magnetic Resonance Spectroscopy in Prostate Treatment Planning, *Int. J. Radiation Oncology Biol. Phys*., Vol. 58, 5: 1577–1583, 2004
12. M. Zaider, M.J. Zelefsky, E.K. Lee, K.L. Zakian, H.I. Amols, J. Dyke, G. Cohen, Y.C. Hu, A.K. Endi, C.S. Chui and J.A. Koutcher, Treatment Planning for Prostate Implants Using Magnetic-Resonance Spectroscopy Imaging, *Int. J. Radiation Oncology Biol. Phys.*, 47(4): 1085–1096, 2000
13. T. Mizowaki, G. Cohen, A.Y. Fung, and M. Zaider, Towards Integrating Functional Imaging in the Treatment of Prostate Cancer with Radiation: The Registration of The MR Spectroscopy Imaging to Ultrasound/CT Images and Its Implementation in Treatment Planning. *Int J Radiat Oncol Biol Phys.*, 54(5):1558-64, Dec 2002
14. J. Xuan, Y. Wang, T. Adal, Q. Zheng, W. Hayes, M.T. Freedman, and S.K. Mun, A Deformable Surface-Spine Model for 3D Surface Registration, *International Conference on Image Processing*, 3:236 - 239, Oct 1997

15. A. Bharatha, M. Hirose, N. Hata and S. K. Warfield, M. Ferrant, K.H. Zou, E. Suarez-Santana and J. Ruiz-Alzola, A. D'Amico, and R. A. Cormack, R. Kikinis, F.A. Jolesz, and C.M.C. Tempany, Evaluation of Three-Dimensional Finite Element-Based Deformable Registration of Pre- and Intraoperative Prostate Imaging, *Med. Phys.*, 28(12): 2551-2560, 2001
16. M. Ferrant, O. Cuisenaire, and B. Macq, Multi-Object Segmentation of Brain Structures in 3D MRI Using a Computerized Atlas, *in SPIE Medical Imaging '99*, 3661-2: 986–995, 1999
17. J. Crouch, S. Pizer, G. Mageras, G. Cohen, M. Zaider, S. Joshi, and E. Chaney, Validation of A Method for Non-Rigid Registration of Prostate Images Using Finite Element Analysis, *Second International Conference on Translational Research*, March 2003
18. A. Mohamed, C. Davatzikos, and R. Taylor, A Combined Statistical and Biomechanical Model for Estimation of Intra-Operative Prostate Deformation, *MICCAI*, 2489: 452-460, November 2002
19. F. L. Bookstein, Principal Warps: Thin-Plate Splines and the Decomposition of Deformations, *IEEE Transactions on Pattern analysis and Machine Intelleigence*, 11(6): 567-585, 1989
20. R. Wu, K.V. Ling, W. Shao, and W.S. Ng, Registration of Organ Surface with Intra-operative 3D Ultrasound Image Using Genetic Algorithm. *International Conference on Medical Image Computing and Computer-Assisted Intervention (MICCAI'03)*, 2878: 383-390, 2003
21. W. Shao, R. Wu, K.V. Ling, C.H. Thng, H.S.S. Ho, C.W.S. Cheng, and W.S. Ng, Evaluation of A Surface-To-Volume Registration Method for Prostate Gland and Its Application to Ultrasound Image Segmentation, *IEEE International Workshop on Biomedical Circuit & Systems*, S3.7.INV: 19-22, Dec 2004
22. M. Mitchell, *An introduction to genetic algorithm*, Cambridge, Mass. MIT press, 1996
23. P. J. Besl and N.D. McKay, A Method for Registration of 3-D Shapes, *IEEE Transactions on Pattern Analysis and Machine Intelligence*, 14(2): 239 -256, 1992
24. R.L. Harder and R.N. Desmarais, Interpolation Using Surface Splines, *J. Aircraft*, 9: 189-191, 1972
25. A. Goshtasby, Registration of Images with Geometric Distortions, *IEEE Transactions on Geoscience and Remote Sensing*, 26(1): 60-64, 1988
26. G. Wahba, Spline Models for Observational Data. *CBMS-NSF Regional Conference Series in Applied Mathematics*, 59: SIAM, 1990.
27. P. Thompson and A.W. Toga, A Surface-Based Technique for Warping Three-Dimensional Images of the Brain, *IEEE Transactions on Medical Imaging*, 15(4): 402-417, Aug 1996
28. R.H. Davies, C.J. Twining, T.F. Cootes, J.C. Waterton, and C.J. Taylor, 3D Statistical Shape Models Using Direct Optimization of Description Length, *ECCV'02*, 2352: 3-20, 2002
29. C.R. Meyer, J.L. Boes, P.H. Bland, K.R. Zasadny, P.V. Kison, K. Koral, K.A. Fray, and R.L. Wahl, Demonstration of Accuracy and Clinical Versatility of Mutual Information for Automatic Multimodality Fusion Using Affine and Thin-Plate Warped Geometric Deformations, *Medical Image Analysis*, 1(3): 195-206, 1997